MATERIALS PHYSICS AND MECHANICS RESEARCH ARTICLE

Submitted: July 3, 2024 **Revised: September 11, 2024** **Accepted: September 23, 2024**

Thermal analysis of wear of polymer-polymer friction pairs in vacuum and atmosphere conditions

A.O. Pozdnyakov [1,2] ✉, **E.B. Sedakova** [2]

[1] Ioffe Institute, Saint-Petersburg, Russia

[2] Institute for Problems in Mechanical Engineering of RAS, Saint-Petersburg, Russia

✉ ao.pozd@mail.ioffe.ru

ABSTRACT

A study of friction and wear of polyoxymethylene-polyoxymethylene and polytetrafluoroethylene-polytetrafluoroethylene pairs with simultaneous registration of the level of heating caused by friction has been carried out. The data obtained were analyzed both by using the energetic wear versus friction power plots and by using the solutions of finite element simulations of the thermal problem in the realistic friction geometry of the thrust bearing type used in the experiments. The solutions provide estimates of heating in vacuum and atmosphere. The calculated heating levels in vacuum suggest that triboinduced scissions of polyoxymethylene macromolecules registered by means of mass-spectrometry in polyoxymethylene-polyoxymethylene pair are initiated at temperatures below the temperatures of the onset of pure thermal decomposition of this polymer and its melting. Correlation between the presence of triboinduced scissions of macromolecules upon friction force transition, the registered exponential growth of wear upon increase of friction power in polyoxymethylene-polyoxymethylene pair and the absence of these phenomena in other pairs studied suggests that triboinduced scissions of macromolecules is governing mechanism controlling overall wear of the polymers studied. The approach was also shown to be informative in comparison of the wear of these polymers against steel and of the wear of pure polyoxymethylene and its composite with C_{60} fullerene.

KEYWORDS

polymer • polymer composite • sliding surface temperature • friction pair • friction force • friction work wear resistance • vacuum • convection • mass-spectrometry • plastic deformations • polyoxymethylene polytetrafluoroethylene • glass transition temperature

Citation: Pozdnyakov AO, Sedakova EB. Thermal analysis of wear of polymer-polymer friction pairs in vacuum and atmosphere conditions. *Materials Physics and Mechanics*. 2024;52(4): 63–80. http://dx.doi.org/10.18149/MPM.5242024_7

Introduction

The wear process of polymers and their composites is an important practical problem [1–3]. Its experimental study consists of measurements of the main interrelated parameters: friction force (F_{fr}), normal load (F_n) or nominal pressure ($P = F_n/S$, where S is a nominal contact area), relative sliding speed of rubbing bodies (V) and the value of sample mass loss (Δm). Important parameter in wear studies is a proportionality coefficient, usually called "energetic wear", between Δm and the total work spent by friction forces during the experiment $I = \Delta m/A$ ($A = \int_0^L F_{fr} \cdot \mathrm{d}x$, where x is the current path length, L is the total friction path length). In the case of polymer materials, the role of heating is significant, due to the strong dependence of their properties on temperature. Therefore, the account of the triboinduced heating of the samples (ΔT) is needed in relation to the above parameters. Our previous works [4,5] have shown that I measured in polyoxymethylene (POM)-POM symmetric pair exponentially increases with increasing parameter $P \cdot V$. This

Publisher: Peter the Great St. Petersburg Polytechnic University

parameter is found in the analytical solution of diffusion equations describing heating level at the interface between two semi-infinite bodies in perfect contact (see, e.g. [6]):

$$\Delta T = \frac{2 \cdot J}{\lambda} \cdot \sqrt{\frac{k \cdot t}{\pi}}, \quad (1)$$

where J is the energy flow into one of the contacting bodies, $k = \frac{\lambda}{\rho \cdot C_v}$ is the thermal diffusivity coefficient, λ is the thermal conductivity coefficient, ρ is the density, C_v is the specific heat capacity, t is time.

In [4,5] we used this equation to qualitatively judge on the trends in heating level at the interface. However, the conditions necessary to obtain the analytical solution (1) are the time-independent magnitude of the heat source during friction (specific friction power): $W = F_{fr} \cdot V/S = \mu \cdot F_n \cdot V/S = \mu \cdot P \cdot V$ = const (μ is the coefficient of proportionality of the one-term Amonton-Coulomb law: $F_{fr} = \mu \cdot F_n$, usually called the friction coefficient) and the constancy of the thermal properties of the bodies (k = const). Note, the value of W is thus equal to $P \cdot V$ parameter with an accuracy to multiplier μ. The distribution of friction power in counter body (1) and (2) is described by: $J_1 = W \cdot k_d$, $J_2 = W \cdot (1 - k_d)$, where J_1 and J_2 are flows into the bodies (1) and (2), respectively [6], k_d is the heat distribution coefficient. In real dynamic friction experiments, F_{fr} and k (see e.g. [7]) depend on sliding time at a constant F_n. Equation (1) also does not take into account heat removal by convection and radiation and thus cannot be used for long-term friction. Convection heat loss is obviously significant during friction under atmospheric conditions and is negligible in vacuum conditions. Note also that the measurements of the temperature directly at the interface is a complex experimental problem. In this regard, for real experimental conditions where the bodies of specific finite sizes and material properties are used, it is necessary to develop computational approaches that take into account the factors discussed above. Recently, the analysis of thermal problems in friction were actively carried out by using numerical methods [8–16], including the finite element method (FEM). Many studies address the solution of the inverse thermal problems in friction with at least partial account of experimental parameters (see [11] and references therein), however the relation of tribogenerated heating to polymer wear has not been sufficiently explored in recent works, though the problem was formulated in earlier studies [17].

Our studies suggest [4,5] that the scissions of macromolecules are a reason of friction force transitions from low to high level in POM-POM pair and determine the wear of the polymer. Quantitative analysis of the interrelations between transformations of macromolecules and macroscopic wear as well as understanding of the nature of these interrelations require quantitative estimates of triboinduced heating of the friction interface in the real experimental geometry. The purpose of our work is, therefore, to adapt FEM analysis to the real experimental friction geometry we are using (thrust bearing) in order to account for heat generation at friction interface and its removal by convection in the analysis of wear of model polymer-polymer friction pairs in atmosphere and vacuum conditions. The attempt is done to apply the results of simulations to the interpretation of experimental data on wear of symmetrical friction pairs polytetrafluoroethylene (PTFE)-PTFE and POM-POM. A qualitative comparison of these data with the data obtained in the case of friction of these polymers against steel was also carried out. An analysis of these issues for such friction pairs has not been found in the

literature, despite the ongoing theoretical and practical interest in this problem [18–23]. The study is important, among other things, because the friction of polymer against polymer is also realized in the case of friction of polymers against inorganic surfaces, e.g. metals, due to the formation of polymer transfer layers on their surface.

Materials and Methods

To determine F_{fr} and Δm under atmospheric conditions, a friction machine of our own design was used. The machine realizes friction in thrust sliding bearing geometry [4]. Figure 1 is a drawing of the unit that implements friction. It consists of a steel rod (1), located in the motor gearbox, driven by three-phase motor. A hollow cylinder-counterbody made of polymer (2) is tightly installed into the top face of the rod. A flat polymer or steel plate counterbody (3) fixed at steel table holder surface (4) is loaded onto the top of the hollow cylinder by normal load. The table with the plate is fixed on the top of the gyroscopically adjusted rod (5), which rotates freely in zirconium oxide rolling bearings (6). The rotation of the table (4) and rod (5) caused by the friction of the hollow cylinder, loaded onto flat plate-counterbody and rotating around its axis, is restrained by a rigid thin steel rod (not shown). One end of this thin rod is fixed at the outer radius of the table (7), and the other on a strain gauge beam (not shown).

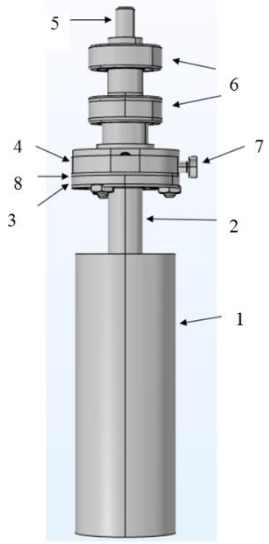

Fig. 1. General view of the friction unit implementing friction. Rotating steel rod (1), hollow cylinder counterbody (2), plate counterbody (3), steel table holder (4), rotating steel rod (5), zirconium oxide bearings (6), screw-holder (7) of the thin rod (see text) connecting the table-holder and the strain gauge beam thus constraining rod (5) from rotation, electrical and heat-insulating paper layer (8)

The force measured by the strain gauge beam is proportional to the torque created by friction [4]. This enables calculation of the friction force F_{fr} from the given radius of the outer side of the table-holder, inner and outer radii of the friction generated ring at the plate counterbody (with an accuracy of 0.1 mm the latter radii corresponded to the radii r_1 and r_2 of the hollow cylinder [4]). The table holder is covered with an electrical and thermal insulating layer of paper of around 0.5 mm thickness (8), located between

the plate (3) and the table (4). Due to its low thermal conductivity, the presence of this insulating layer increases sensitivity of the measurements of small absolute values of temperature. The flat plate is fixed to the holder table by using screws. The compression force of the tightening screws was not quantitatively measured in different experiments (this is typical for majority of the works in tribological practice). This may lead to deviations of, e.g., the thermal diffusivity of the paper layer from the value used in the calculations (Table 1).

Table 1. Material properties used in calculations

	POM	PTFE	Steel 20	Paper
ρ, kg/m^3	1410.00	2200.00	7900.00	500.00
C_v, J/kgK	1470.00	1500.00	420.00	1340.00
λ, W/(m·K)	0.31	0.167÷0.300	45.00	0.04
$k = \frac{\lambda}{\rho \cdot C_v}$, m^2/sec	$1.49 \cdot 10^{-7}$	$9.95 \cdot 10^{-7}$	$1.35 \cdot 10^{-5}$	$6.00\ (\pm 2.00)\ 10^{-8}$ (see text)
T_g^*, K	182.00 [24]	160.00 [24] 140.00 ÷ 400.00 [25]		
T_m^{**}, K	442.00	600.00	1790.00	
σ_o^{***}, MPa	140.00	50.00	1000.00	

* glass transition temperature

** melting temperature

*** Brinell hardness

The counterbodies are hollow cylinders with a height of 18 mm, external (r_1) and internal (r_2) radii of 4.5 and 3 mm and plates with a thickness of ~ 1–2 mm and lateral dimensions of ~ 15 × 20 mm. They were cut from industrial PTFE (PKP, Polimerkhimprom™), POM (POM-H Ticona™) and grade 20 steel (GOST 1050-88) material. POM-fullerene C_{60} composites were prepared by introducing a saturated solution of C_{60} in toluene into the polymer melt with constant mechanical stirring of the mixture for several minutes at a temperature of ~ 200 °C. Fullerene C_{60} powder with a concentration of C_{60} > 99 wt. % was used (Fullerene Technologies company). After mechanical mixing of the components, the melt was cast onto glass substrate, subjected to compression between two glass plates under a pressure of ~ 5 MPa and non-isothermally cooled to room temperature. The degree of dispersion of fullerene in the composite was not controlled at this stage of research. It can be noted that the resulting composites had a darker, light ochre color compared to the white color of the original POM. The fullerene concentration in the composite was ~ 0.5 mass. %.

The contact surfaces of the samples were grinded to a roughness of R_a ~ 0.5 μm, determined with a TR-200 profilometer. Before rubbing, the samples were washed with warm distilled water and dried. Friction started at room temperatures (T_{amb}) at atmospheric humidity ~ 50 %. The mass loss Δm of the samples as a result of friction was determined using Kern 770 analytical balances as the difference in the mass of the sample (both the hollow cylinder and the plate were weighed) before and after friction. Before weighing, the samples were carefully wiped with a clean, dry calico cloth to remove wear particles. The presence of the particles was controlled by using an optical microscope. The accuracy of determining the mass of samples is 0.1 mg. Experiments

were carried out in the range of loads F_n up to 150 N (contact pressure up to ~ 4 MPa, for the nominal contact area $S = \pi \cdot (r_1^2 - r_2^2)$ and sliding speeds up to 0.11 m/s. The temperature during friction was measured with a chromel-alumel thermocouple. The tip of the thermocouple is tightly clamped between a flat, stationary plate counterbody and an insulating paper layer located at the surface of sample holder table. The distance between the friction interface and the measuring point used in the calculations is thus estimated as the thickness of the plate counterbody in the given experiment. The accuracy of lateral position of the thermocouple tip is estimated at the level of ~ 1 mm. The values of material properties [23,24] used in FEM simulations are given in Table 1. Experiments in vacuum conditions of mass-spectrometer were earlier performed by using the friction unit of the same geometry and properties. Experiments in mass-spectrometer are discussed elsewhere [4] in more detail.

Results and Discussion

Statistics of Δm values was collected in experiments carried out in atmosphere for sliding speed V range of 0.021 ÷ 0.1 m/sec (calculation based on the average radius of a hollow cylinder $0.5 \cdot (r_1 + r_2)$) and P values in the range of 0.39 ÷ 3.6 MPa. Comparable statistics of around 20 measurements was collected for all pairs. Figure 2(a) shows the experimental points corresponding to all experiments performed, presented in double logarithmic coordinates $\Delta m \div A$ (A is the total work of friction in the given experiment). Hollow circles show the results obtained for the PTFE-PTFE pair, gray circles - for the POM-POM pair. Data for steel-PTFE and steel-POM pairs are shown as solid and hollow squares, respectively. It can be seen that when the experimental parameters change in the same range of P and V values, the data for the POM-POM pair have an order of magnitude greater scatter compared to the PTFE-PTFE, steel-PTFE and steel-POM pairs. For PTFE-PTFE, steel-PTFE and steel-POM pairs, the dependences of Δm on A are quite satisfactorily fit by linear functions (straight lines 1,2,3). In the case of the POM-POM pair, the scatter of data does not allow us to identify a general linear dependence for all combinations of P and V. Note, however, that for fixed P and V, the dependences of Δm on A in the POM-POM pair has much smaller scatter, similar to that recorded in the PTFE-PTFE pair, and can also be described by similar linear relationships which are not shown in the figure for view convenience of the data. They shift upwards upon growth of W. These observations make it reasonable to plot the value of the proportionality coefficient between these values ($I = \Delta m/A$) versus the value of the friction power W. These plots (Fig. 2(b)) show that for the POM-POM pair the value of I increases exponentially upon the growth of the value of W. For POM-POM pair friction coefficient is ~ 0.35 for the data shown in Fig. 2. This level of μ is detected after friction force transition $F^{min}_{fr} \longrightarrow F^{max}_{fr}$ in POM-POM pair (see below in Fig. 4(a) and other examples in [4,5]). Before $F^{min}_{fr} \longrightarrow F^{max}_{fr}$ transition in POM-POM pair the value of μ is ~ 0.1, close to that for other pairs studied. In these pairs no transition of friction force was detected in our dynamical friction force measurements. The mass loss of the samples at the level of friction force corresponding to μ ~ 0.1 in POM-POM pair is below sensitivity level of analytical balances (± 0.1 mg). The increase in the value of I with increasing W for the pairs PTFE-PTFE, steel-PTFE and steel-POM is not obvious.

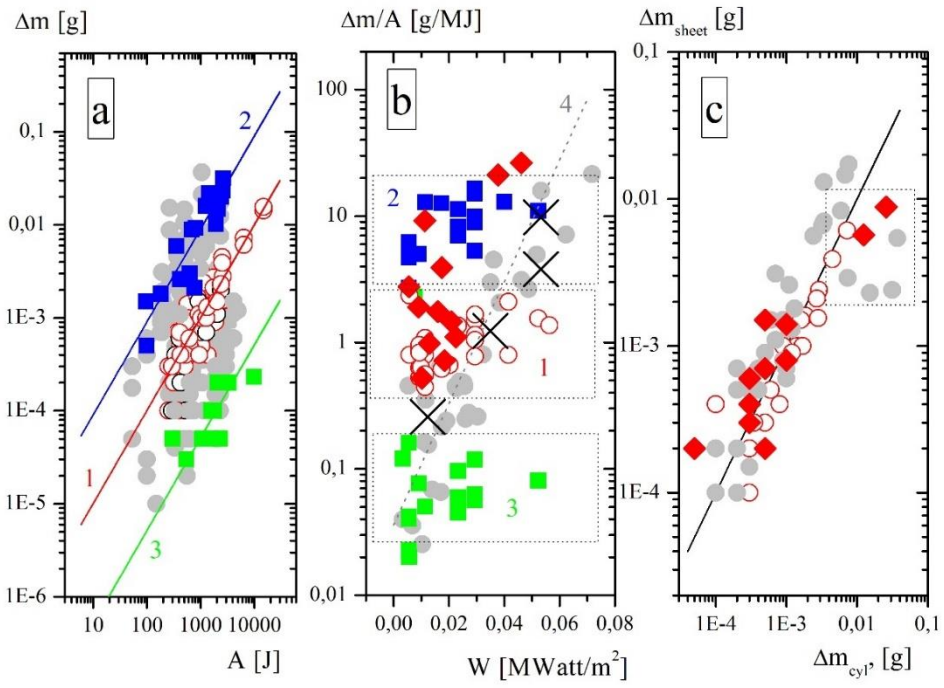

Fig. 2. (a) Dependences of Δ*m* on the friction work (*A*) for experiments carried out for all combinations of *P* and *V*. Gray solid circles: POM-POM friction pair. Open red circles: PTFE-PTFE pair (line 1), solid blue squares: steel-PTFE pair (line 2), solid green squares – steel-POM pair (line 3). Double logarithmic coordinates are used; (b) dependences of the magnitude of coefficient Δ*m/A* on the magnitude of *W* for friction pairs PTFE-PTFE (box 1, open red circles), steel-PTFE (box 2, solid blue squares), steel-POM (box 3, solid green squares), POM-POM (gray solid circles around line 4). Crosses: data from experiments with the POM-POM-C_{60} pair. Solid red rhombs: POM-POM friction pairs in a vacuum. The ordinate axis is logarithmic. For symmetric POM-POM and POM-POM-C_{60} pairs the mean values of Δ*m* of cylinder and plate counter bodies are plotted; (c) dependences of the mass loss of the stationary plate (Δm_{plate}) versus the mass loss of the cylinder (Δm_{cyl}). Gray solid circles: POM-POM pair. Open red circles: PTFE-PTFE pair. Solid red rhombs – friction experiments with POM-POM pairs in a vacuum. Double logarithmic coordinates are used

The average *I* values for these pairs were, respectively, 0.99 ± 0.02 g/MJ (PTFE-PTFE), 9 ± 0.7 g/MJ (steel-PTFE), and 0.03 ± 0.005 g/MJ (steel-POM).

Crosses in Fig. 2(b) show the measurements carried out at different *W* for the POM-C_{60} composite upon friction against POM. It can be seen that, within the range of experimental scatter, the difference between the values of *I* of pure POM and POM-C_{60} composite is difficult to distinguish. It can be assumed that the similar wear values of the composite and pure POM are due to the strong aggregation of fullerene in the matrix as a consequence of the method of mixing the components we used. Further efforts are underway to deal with the problem.

Figure 2(c) shows the dependences of the mass loss of the stationary plate (Δm_{plate}) versus mass loss of the cylinder (Δm_{cyl}) for the described experiments. The straight line in Fig. 2 shows the dependence for equal values of mass loss of the counterbodies: $\Delta m_{plate} = \Delta m_{cyl}$. It is seen that for the PTFE-PTFE pair, the experimental points (hollow circles) are located near this dependence. This implies even wear of plate and cylinder in

this pair. In the case of POM-POM pair, the experimental points obtained for $W < 0.03$ MW/m^2 are also located around this dependence, thus indicating even wear of the plate and the cylinder at low friction powers. However, for $W > 0.03$ MW/m^2 (points highlighted by the box in Fig 2(c)), the measurements show strong increase in wear of the POM cylinder compared to wear of POM plate. Similar results were obtained in the case of POM-POM friction in vacuum (solid red rhombs highlighted by the box in Fig. 2(c)). Note here that for these vacuum experiments with POM-POM pair (solid red rhombs in Fig. 2(b)), the values of I are located above the characteristic exponential dependence of I versus W for the POM-POM friction pair under atmospheric conditions (line 4). This suggests higher heating at friction interface due to the absence of heat removal by convection in vacuum. For other pairs the $I \div W$ dependences in $P{\cdot}V$ range accessible in our vacuum friction machine ($P{\cdot}V$ up to ~ 0.15 MPa·m·sec^{-1}) were comparable in vacuum and in atmosphere. Recall, the value of W is equal to more widely used in practice $P{\cdot}V$ parameter with an accuracy to multiplier equal to friction coefficient μ.

The experimental data described above qualitatively suggest that growth of W and hereto related increase in heating in the POM-POM pair result in transition from even wear of the cylinder and the plate to increased wear of the cylinder compared to the plate. This effect is not observed in the PTFE-PTFE pair in the range of W studied. This suggests that tribogenerated heating does not result in uneven wear in this pair and does in POM-POM pair. The small and comparable scatter of the $\Delta m \div A$ dependences for the steel-POM and steel-PTFE pairs may also indicate a negligible effect of heating on wear in these friction pairs.

As shown in [4,5], the mechanism of POM wear in the thermodynamically compatible POM-POM pair is reasonably interpreted by triboinduced scissions of POM macromolecules in a shear field. By using mass-spectrometry it was shown [4] that the scissions initiate $F^{min}_{fr} \rightarrow F^{max}_{fr}$ transition in POM-POM pair. For PTFE-PTFE, steel-PTFE and steel-POM and other POM-polymer pairs studied in [4], neither friction force transitions nor macromolecular volatile products of scission are recorded at comparable initial W levels. This is in good accord with the absence of changes in I upon growth of W level in PTFE-PTFE pairs, steel-PTFE and steel-POM pairs (see above discussion of Fig. 2(b)). The exponential dependence of I on W in the POM-POM pair measured after $F^{min}_{fr} \rightarrow F^{max}_{fr}$ transition covers the range of I in all three other pairs studied (highlighted by boxes in Fig. 2(b)). The effects described above make a more detailed quantitative analysis of tribogenerated temperatures at the friction interface important and is considered below.

Simulation method and Discussion

To calculate tribo-induced heating (ΔT), preliminary modeling of the friction geometry of the friction unit (Fig. 1) used in the work has been carried out. The main part of the unit, which realizes friction *per se* in the geometry of the thrust bearing, is shown in Fig. 3(a). Simplifications made to construct the model shown in Fig. 3(a) were justified by the following factors. In real friction geometry, zirconium oxide ball bearings (6 in Fig. 1), located in a lining of the same material, do not move when friction experiments are performed and have very low thermal conductivity. The area of their contact with the bearing lining is also vanishingly small compared to the contact areas of other objects in

the model. In this regard, they were not used in the calculation geometry used. Calculations also show that the increase of the size of steel rods (1,5 in Fig. 1) above that used in simulations described below led to negligible (at the level of 1 K) changes in the resulting temperature dependencies. Account of small machine parts of the real drawing (Fig. 1) resulted in negligible changes to these dependencies and were not modeled.

Mathematically, heating processes can be described by solutions of non-stationary diffusion equation of the form [26]:

$$\frac{\partial T}{\partial t} - k \cdot \nabla^2 T = 0, \quad (2)$$

with given boundary and initial conditions. The equation assumes infinite heat propagation velocity and serves as first approximation for more realistic models [27]. To analyze the thermal problem, we developed calculation programs in the *Comsol Multiphysics6.2™* software package for numerical calculations using FEM [28,29] based on Galerkin type methods [30]. Its use greatly simplifies the analysis of three-dimensional temperature distributions in contacting bodies and the time dependences of ΔT. To analyze the thermal problem in the geometry discussed above, the *Heat Transfer in Solids* simulation block was used, which implements the solution of Eq. (2) using FEM, in combination with the non-stationary simulation block *Time Dependent Study*. Geometric regions were meshed into a grid of tetrahedrons with their size decreasing near the interface by using the procedure of creating boundary layers. The boundary conditions associated with heat transfer by convection were specified at all surfaces of the objects constituting the geometry except their ends. Note, heat fluxes by radiation constituted a small fraction of the total flux, therefore this heat removal channel was not directly taken into account in the calculations. However, it is implicitly included in the total heat removal, taken into account by the effective convective heat removal coefficient (see below).

FEM calculations using realistic experimental geometry were preliminary compared to analytical solutions of model thermal problems. For a one-dimensional diffusion equation for two semi-infinite bodies in perfect planar contact, with a time-independent energy flow J at the interface ($J = -\lambda \cdot \frac{\partial T(0,t)}{\partial z}$), the analytical solution for the temperature distribution in the direction perpendicular to the interface has the form [6]:

$$\Delta T = \frac{2 \cdot J}{\lambda} \cdot f(q) \cdot \sqrt{\frac{k \cdot t}{\pi}}, \quad (3)$$

where $f(q) = e^{-q^2} - 2 \cdot q^2 \cdot \int_1^\infty d\eta \cdot e^{-\eta^2 \cdot q^2}$, $q = \frac{z}{\sqrt{4 \cdot k \cdot t}}$, z is the coordinate in the direction perpendicular to the interface, J is the heat flow into one of the contacting bodies. This ideal geometry obviously does not account for convective and radiative fluxes. In Fig. 3(b), curve 1 shows the calculation obtained by using FEM for the case of contact between the flat top ends of two identical solid cylinders (their full length is the same as the length of the full realistic geometry, radius 10 mm, that is maximum radius in real geometry) made of POM without account for heat removal by convection. Calculation parameters used are mean value of F_{fr} from friction force dependence in Fig. 4(a) (27 N), heat distribution coefficient $k_d = 0.5$ and time of friction 900 sec. This simplifies comparison with experimental data analysis of symmetric pairs. This profile reflects

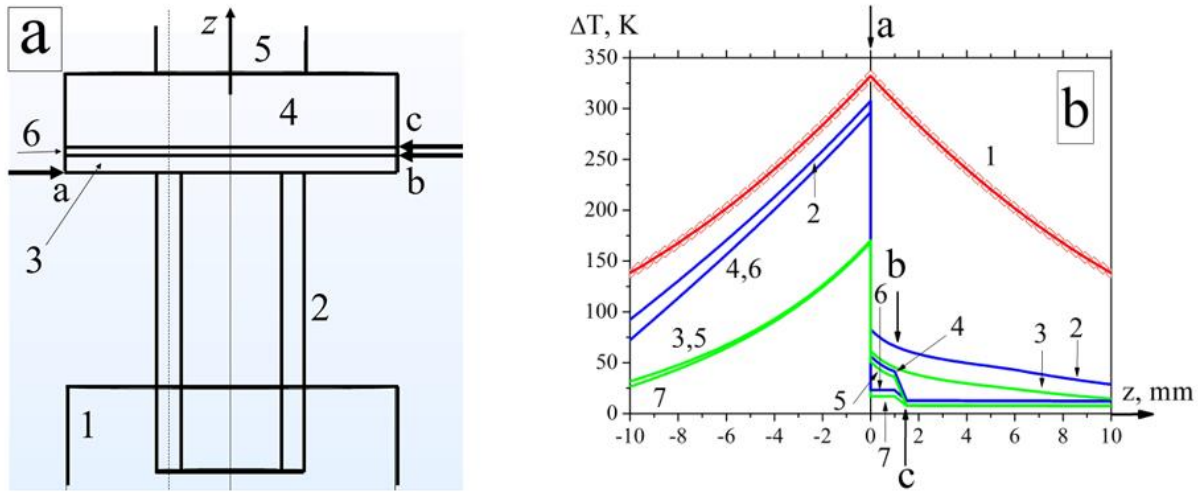

Fig. 3. (a) Side view of the geometry of the friction unit used in FEM simulations. Steel rod (1), hollow cylinder made of PTFE or POM (2), plate counterbody made of POM, PTFE or steel (3), steel table-holder (4), located on a freely rotating steel rod (5), paper insulating layer (6). Radii of cylinder rod (1) and table table holder (4) used in calculations are: r_o = 10 mm. Size of the hollow cylinder (2): height 18 mm, outer (r_1) and inner (r_2) radii: 4.5 and 3 mm, thickness of the counterbody plate 1 mm, thickness of the insulating layer 0.5 mm. The depth of insertion of the hollow cylinder into the rod is 5 mm. The length of the rod (1) and cylinder (5) used in the calculations was chosen to be equal to 70 mm; (b) temperature distribution profiles along the *z* axis shown in fragment (a). 1 is the profile obtained by using FEM without a heat removal for a model of two identical solid POM cylinders with a radius r_o = 10 mm in contact of their flat top ends. The open rhombs around curve 1 show the analytical solution obtained using Eq. (3) (F_{fr} = 27 N, *t* = 900 sec in both calculations, see text). Profiles 2–7 were obtained for real geometry given by the fragment (a) along dashed curve located at the center of the edge of the hollow cylinder (see text). Profiles 2 (blue), 3 (green) – all machine parts have POM material properties, *h* = 0 Watt/(m^2·K)), 3 – *h* = 8 Watt/(m^2·K), respectively. Profiles 4 (blue),5 (green) – machine parts have material properties of real friction unit, friction pair POM-POM, *h* = 0 Watt/(m^2·K) and *h* = 8 Watt/(m^2·K), respectively. Profiles 6, 7 the same for friction pair POM (cylinder)-steel (plate), *h* = 0 Watt/(m^2·K), *h* = 8 Watt/(m^2·K), respectively. Arrows a, b, c show the interfaces between the cylinder and the plate, between the plate and the insulating layer, between the insulating layer and the steel table-holder, respectively

the temperature distribution in the center of the solid cylinders along z axis (Fig. 3(a)). Points in Fig. 3(b) show the solutions obtained by using Eq. (3). It can be seen that the analytical solutions agree with the results of FEM simulations with high accuracy. Near the ends of the cylinders, that is, at a considerable distance from the friction interface, slight deviations from analytical solutions are observed (not shown).

The temperature distributions along the radius of a solid cylinder obtained in FEM simulations were also analyzed. Boundary conditions at the surfaces of objects caused by heat removal by convection are described by relation: $\lambda\,(dT/dn)_{n=o} = -h\cdot(T_{n=0}-T_{amb})_{n=o}$, where *n* is the value of the corresponding coordinate, and the origin of coordinates is associated with the boundary, *h* is the heat removal coefficient [27]. They were compared to the analytical solution for the temperature profile along the radius of the cylinder of infinite length cooled by convective heat removal from external surfaces characterized by heat removal coefficient *h* (the solution of the diffusion equation by the method of separation of variables is described, e.g., in [27]):

$$\theta = \theta_o \cdot \sum_{n=1}^{\infty} \frac{2\cdot J_1(\mu_n)}{[J_o(\mu_n)^2+J_1(\mu_n)^2]} \cdot J_o\left(\mu_n \cdot \frac{r}{r_o}\right) \cdot exp\left(-\mu_n^2 \cdot \frac{k\cdot t}{r_o^2}\right), \quad (4)$$

where t is time, $\theta = T(t,r) - T_{amb}$ and $\theta_o = T_{init} - T_{amb}$ are the current and initial temperatures relative to the ambient temperature T_{amb}, respectively, $T(t=0,r) = T_{init}$ is the condition of the same temperature over the entire cylinder prior to cooling, J_o and J_1 are Bessel functions of the zero and first order, respectively, μ_n are parameters determined graphically by solutions of the equation $\frac{J_o(\mu)}{J_1(\mu)} = \frac{\mu}{Bi}$, $Bi = \frac{h \cdot ro}{\lambda}$ (*Biot* number), r_o is the radius of the cylinder, r is the distance from its center along the radius. In this case, the dome-shaped profiles (not shown) of the ΔT distribution along the radius of the cylinder with the maximum ΔT in its center calculated by using FEM coincided with the analytical solutions (Eq. (4) with four series number was used) with the same high accuracy as in the example of ΔT profiles along the cylinder axis discussed above. The mesh parameters of the geometry used in the above model FEM calculations were applied in the calculations of the real geometry (Fig. 3(a)) used for fitting the experimental ΔT dependences reported below.

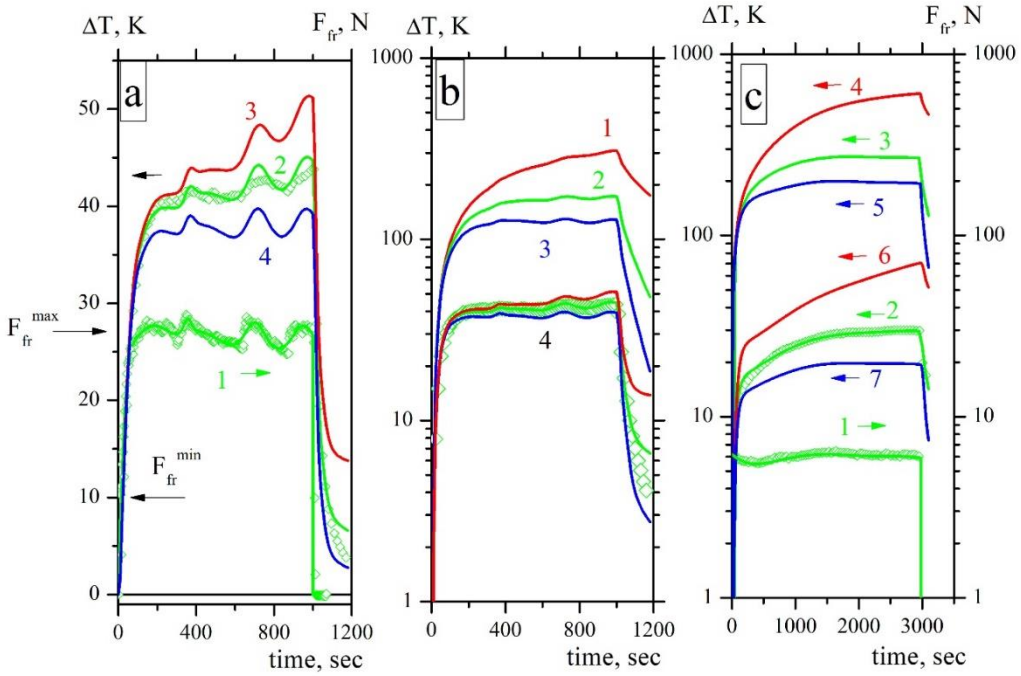

Fig. 4. (a) Example of synchronous measurements of friction force (open green rhombs 1 with an arrow in the direction of the right axis) and temperature (open green rhombs 2) for a POM-POM friction pair. Curve 1 shows the approximation of the experimentally measured dependence $F_{fr}(t)$ used in FEM calculations. Curve 2 shows the FEM calculation of heating at the measurement point for h = 8, red curve 3 for h = 0 Watt/(m^2·K), blue curve 4 for h = 16 Watt/(m^2·K). Friction conditions: V = 0.021 m/sec, F_n = 72 N. The signal recording step used is ~ 0.5 sec. The thickness of the counterbody plate is ~ 0.5 mm; (b) FEM prediction of the level of heating at the friction interface on the side of hollow cylinder (Fig. 3(b)) for the same experiment as that used in the fragment (a). Red curve 1: h = 0 Watt/(m^2·K), green curve 2: h = 8 Watt/(m^2·K) (curve 2), blue curve 3: h = 16 Watt/(m^2·K). Curves in area 4 are curves 2,3,4 from the fragment (a); (c) example of synchronous measurements of friction force (open green rhombs 1) and temperature (open green rhombs 2) for a PTFE-PTFE friction pair. Green curve 3: FEM prediction of heating level at the friction interface on the hollow cylinder side (Fig. 3(b)) for h = 8 Watt/(m^2·K), red curve 4: h = 0 Watt/(m^2·K), blue curve 5: h = 16 Watt/(m^2·K). Curves 6 and 7: simulated heating level at the measurement point for h = 8 Watt/(m^2·K) and h = 16 Watt/(m^2·K), respectively. Friction conditions: V = 0.11 m/sec, F_n = 72 N. Counterbody plate thickness ~ 1.5 mm

Curves 2–7 in Fig. 3(b) show the calculated ΔT profiles along the cylinder axis for a real friction unit. In this case, shown are profiles along a line located at the center of the edge of the hollow cylinder at radius $r = (r_1+r_2)/2$ parallel to the axis z. The calculation for $F_{fr}(t)$ dependence for POM-POM pair presented in Fig. 4(a,b) for time of friction of 900 sec is used for illustration. Arrows a, b, c in Fig. 3(b) indicate locations of friction interface, the interface between the plate-counter body and the insulating layer, the interface between the layer and the surface of steel sample holder, respectively. The initial condition in the calculations was chosen to be constant temperature of all objects in the model, equal to the ambient temperature (T_{amb}, in the calculations it is set as the initial temperature prior to onset of friction). The boundary conditions in the calculations were the function of the power of the plane heat source at the friction interface ($W(t) = F_{fr}(t)\cdot V/S$) determined from the experimentally measured dependence $F_{fr}(t)$ and the heat removal by convection from the outer surfaces of contacting bodies except the ends of the steel rods. The characteristic features of the profiles are typical for all other calculations. In general terms, they reveal lower level of heating for the real geometry even for h=0 $Watt/(m^2\cdot K)$ (curves 2,4,6) compared to ideal geometry consisting of 2 solid POM cylinders (curve 1). This is due to the presence of steel mechanical parts with high thermal conductivity (rods and plate holder, Fig. 1) in real geometry. This shows that the use of Eq. (1) strongly overestimates calculated temperatures of our real geometry at large friction times and can be used only for qualitative estimates even in the case of absence of convection. As a reference, profiles 2 and 3 present the calculation of real geometry where all parts of the friction unit have material properties of POM. In real geometry containing steel machine parts in the friction unit (rotating and fixed steel rods, Fig. 1) the profiles have the shape of curves 4,5 for h = 0 Watt/(m^2·K) and h = 8 Watt/(m^2·K). In the case of the same real geometry where plate counterbody has material properties of steel, the profile is more uniform across the thickness of the steel plate counterbody (curves 6,7). The calculations discussed below were carried out for measurement point located at a distance equal to the thickness of the plate, that is at the location of chromel-alumel thermocouple tip firmly clamped between the plate and the surface of the steel table holder covered with insulating layer. Note, in the context of thermal problem considered, the role of insulating layer is to increase the ΔT level within the plate, thus increasing the magnitude of the measured level of absolute temperature. In the calculations of symmetric friction pairs, we used the equal distribution of W in upper (1) and lower (2) counterbodies, that is for heat distribution coefficient k_d = 0.5 ($J_1 = J_2 = W/2$) consistent with Sharron formula valid for semi-infinite bodies [31]. This is a reasonable approximation for our calculations of symmetrical friction pair, e.g. POM-POM characterized by nonlinear dependence of I on W (Fig. 2(b)).

In the context of this study another important observation from Fig. 3(b) is the higher temperature level on the side of polymer cylinder compared to that on plate side in our geometry. This difference appears and increases with increasing time of friction. This effect is mainly determined by the difference in the lengths of the polymer cylinder and plate (~ 20 times) in contact with steel rods-holders (Fig. 1). It can also be seen that account of heat removal by convection (h = 8 Watt/(m^2·K)) leads to a decrease in heating levels. They are easily visually discerned Fig. 3(b)) in profiles for different pairs in the area of the plate and less visually discerned in the area of cylinder. The higher level of heating

near the interface on the side of hollow cylinder is in good agreement with the increase of its wear discussed in previous section for high W levels in the POM-POM pair (Fig. 2(c)). The similarity in cylinder and plate wear at low W in POM-POM pair seems to indicate that in this range of W in the POM-POM pair, wear is weakly dependent on the level of heating at the interface. Recall that the absence of the wear growth of the cylinder in the PTFE-PTFE pair (Fig. 2(c)) also indicates negligible effect of heating on PTFE wear in the entire range of W used in this study.

Figure 4 shows examples of heating calculations of two typical temperature measurements in real thrust bearing geometry for the POM-POM (Fig. 4(a,b)) and PTFE-PTFE (Fig. 4(c)) pairs. In these experiments the normal load was the same, the sliding speed velocity V is 5 times higher in the case of PTFE-PTFE pair. Many additional examples of the behavior of friction force exhibiting typical $F^{min}_{fr} \rightarrow F^{max}_{fr}$ transitions (horizontal arrows in Fig. 4(a)) in POM-POM pair [4,5]. At lower W compared to the one shown in Fig 4(a) the $F^{min}_{fr} \rightarrow F^{max}_{fr}$ the path length for transition in POM-POM required to occur increases. For the pairs PTFE-PTFE (Fig. 4(c)), PTFE-steel and POM-steel, no transition is observed in the range of W studied. In these pairs the experimentally measured temperature dependences for these pairs were similar at given W. Note here that it would also be a case in POM-POM pair if this pair would not exhibit $F^{min}_{fr} \rightarrow F^{max}_{fr}$ transitions. The simulations of the experimental dependences for asymmetric PTFE-steel and POM-steel pairs meet the complexities of formulation of the thermal model e.g. discussed below in the text in terms of heat distribution coefficient and are not considered in this paper.

In Fig. 4(a), curve 1 shows a nonlinear approximation (polynomials with an order close to 7 were used) of the experimentally determined $F_{fr}(t)$ (open rhombs) time dependence at constant V. In calculation of $W(t)=F_{fr}(t)\cdot V/S$ required for FEM simulations as a boundary condition, we used average sliding speed at the center of the contact edge $V = \pi\cdot(r_1+r_2)\cdot\upsilon$ (υ[Hz] is a rotation frequency of the hollow cylinder). S was put equal to nominal contact area $S = \pi\cdot(r_1^2-r_2^2)$. It can be seen that the shape of the experimentally measured temperature dependence $\Delta T(t)$ (open rhombs around curve 2) is best fit by simulated temperature dependence (curve 2) obtained for the measurement point (~ 0.5 mm from the friction zone) using a heat removal coefficient value of 8 Watt/(m^2·K) for all objects of the experimental geometry (Fig. 3(a)). This value is close to mean value (h = 8.48 Watt/(m^2·K)) obtained in [23] by calculations of convection problem under assumption of laminar air flow for PTFE samples of the similar shapes and dimensions used in our work as well as in the same friction geometry. It can be also noted that the calculation of cooling after the friction is ceased (the case of cooling the friction joint as a whole unperturbed by friction) best fits the experimental curves also for h = 8 Watt/(m^2·K). The dependence of the calculated temperature at the measurement point for h = 0 Watt/(m^2·K) and h = 16 Watt/(m^2·K) are shown by curves 3 and 4 (Fig. 4(a)), respectively. The value h = 0 Watt/(m^2·K) describes the vacuum conditions with an accuracy to heat removal by radiation. More smooth fitting curves, characterized by reduction in absolute temperature values not exceeding 1 K, can be obtained by twice increase in the lengths of the steel rods 1, 5 (Fig. 3(a)) in the geometry simulated. However, in this work we did not set the task to fully optimize the experimental parameters. This requires complicated study of inverse thermal problem (see, e.g. [11] and references therein). Note

here that Fig. 4(a) shows that the temperature increment at the measurement point during friction in vacuum (h = 0 Watt/(m^2·K), curve 3) compared to the case of friction in atmospheric conditions (h = 8 and 16 Watt/(m^2·K), curves 2,4) is ~ 5–10 K.

The calculations help in quantifying the possible reasons of changes in the experimentally measured heating level at the measurement point for given h. Reference test calculations have shown that the change in the absolute value of ΔT, calculated at the measurement point (located at a distance from the friction interface equal to the thickness of the plate), can reach ~ 10 K when its coordinate changes along the plane of the plate from the center of the hollow cylinder to its edge. Changes in this value related to a possible change in the thermal diffusivity of the insulating paper layer under the plate counterbody upon its mechanical tightening to the table holder by using screws (see discussion in the previous section and Table 1), can also reach ~ 10 K. Increase in the accuracy of measurements would increase the accuracy of calculations of temperature at the measurement point. This can obviously be achieved also by using a more accurate approximations of the experimental dependences $F_{fr}(t)$, more advanced methods of positioning of the thermocouple, account of its inertia [11,14] and, probably, precision in the size of the samples. However, certain differences in the thermal diffusivity of paper insulating layer as a consequence of not yet measured degree of tightening of the screws required for firm fixation of the plate counterbody in each experiment alter the calculated value of maximum ΔT at the friction interface by a value not exceeding one Kelvin.

An additional increase in the accuracy of calculations and fitting procedure can be further achieved by taking into account the dependence of the sliding speed on the radius of the cylinder and the edge effects in contact pressure. The use of smaller time steps in recording temporal evolution of the measured F_{fr} and ΔT is also promising. For example, in a more realistic case of plastic contact of the asperities of rough surfaces, the area of real contact (A_o) can be estimated from the relation: $A_o/S \approx P/\sigma_o$ [6] (plasticity limit in compression or Brinell hardness, σ_o, see Table 1). In our experiments P reaches ~ 4 MPa, i.e. the actual contact area can be a few percent of the nominal one. The friction time of roughness tips of size D ~ 1 μm before leaving the contact is $D/V \sim 10^{-4}$ s. Using relation $J = 0.5 \cdot \mu \cdot \sigma_o \cdot V$ ([6] and references therein), the sufficiently precisive at this short time range, from Eq. (1) we obtain upper estimate of the calculated ΔT of a single flash on a roughness in vacuum at the level strongly below 1 K. The small magnitude of temperature flashes and small heat penetration depths of these flashes into the subsurface layers of around several micrometers [6,32] suggest that they would introduce small high-frequency contribution to our calculation of heating performed by taking into account the nominal contact area. Oscillatory heating behavior (Fig. 4(a)) observed for the POM-POM pair with a characteristic oscillation time around tens of seconds accords well with the behavior of F_{fr} and reflects more smooth processes of tribo-induced structural changes at the interface. Analysis of the complete pattern and accuracy of temperature measurements, including account of wear debris particles, is out of range of this paper. These questions are the subject of ongoing research, in particular with acoustic emission methods since in POM-POM pair the clearly detected noise in acoustic region is detected. It is absent in other pairs studied. This study requires analysis of elastic waves generation which are expected to be in complicated relation to heat flow in the case of mutual sliding of wavy surfaces [33,34].

Curves 1–3 in Fig. 4(b) show the predictive calculation of the temperature versus time dependences at the friction interface on the side of the cylinder (see explanation to profiles in Fig. 3) for h = 0 Watt/(m^2·K), h = 8 Watt/(m^2·K) and h = 16 Watt/(m^2·K). For convenience of comparison, the curves located around experimental points in Fig. 4(b) are the curves 2–4 from Fig. 4(a). From Fig. 4(b) it is seen that the temperature at the interface in vacuum becomes approximately 120 K higher than that in air conditions (h = 8 Watt/(m^2·K)) upon friction. This reasonably explains the increase in energetic wear during friction in vacuum (red solid rhombs, Fig. 2(b)) compared to friction in atmospheric conditions (gray circles, Fig. 2(b)) at the similar levels of W. Sharp increase in ΔT occurs upon friction force transition $F^{min}_{fr} \rightarrow F^{max}_{fr}$ (horizontal arrows in Fig. 4(a)). As is shown in our works [4,5] the transition is accompanied by formation of the tribodecomposition products of POM macromolecules. Note that the amount of tribodecomposition products formed grows with initial level of W [4]. Our suggested mechanism of the formation of tribodecomposition products at these low temperatures is interpenetration of the POM macromolecules across friction interface [4,5], their orientation and scission. Calculations of ΔT in real geometry for various $F_{fr}(t)$ measurements performed at various W (e.g. from data obtained in the vacuum of mass-spectrometer given in [4,5]) show that all the transitions of the friction force $F^{min}_{fr} \rightarrow F^{max}_{fr}$ in the POM-POM pair are initiated at temperatures at the interface not exceeding ~ 50 °C both in atmosphere and vacuum conditions. The formation of decomposition products and the simultaneous increase in the friction force in the POM-POM pair at these temperatures excludes both melting of polyoxymethylene (T_m ~ 170 °C [25]) and the lowest, the less intense, pure thermal decomposition stage of this polymer observed in the thermal decomposition spectra of friction transferred submicron layers of POM at temperatures above 110 °C [4]. Note here that this stage is not yet firmly attributed to the decomposition of intact POM since, due to difficulty of dissolution of POM, thin layers of this polymer could be formed [4] at the substrate only by rubbing POM sample against it. The main stages of thermal decomposition undoubtedly related to decomposition of intact POM start to appear above 200 °C.

The P and V conditions of the experiment in Fig. 4(b) provide estimate of the W value of ~ 0.015 MWatt/m^2 after $F^{min}_{fr} \rightarrow F^{max}_{fr}$ transition (μ ~ 0.35) in POM-POM pair (initial W before transition ~ 0.005 MWatt/m^2), at which the temperature at the interface in air conditions can reach around 170°C, that is the melting temperature of POM. Note that $F^{min}_{fr} \rightarrow F^{max}_{fr}$ transition is also observed for much lower levels of initial W [5]. In the imaginary experiment in vacuum (h = 0 Watt/(m^2·K)) for the same $F_{fr}(t)$ dependence (Fig. 4(b)), the temperature at interface would attain ~ 300 °C (curve 1). Heating calculations for various experimental $F_{fr}(t)$ dependences obtained in vacuum of ~ 10^{-6} Torr for the POM-POM pair (see, e.g., [4,5]) predict heating strongly above 300 °C after the transitions $F^{min}_{fr} \rightarrow F^{max}_{fr}$. These temperatures correspond to the temperatures of almost complete thermal decomposition of thin submicron layers of POM (see the thermal decomposition spectra of friction generated submicron thickness POM layers in [4]). This implies very strong growth of the mass-spectral lines of the thermal decomposition products of POM. However, the simultaneously recorded [4,5] intensity of the formation of POM decomposition products (oxymethylene and trioxane), expected to increase sharply at these high temperatures, on the contrary, reaches saturation and practically does not change with increasing friction time at these high predicted temperatures. The

ratio of oxymethylene and trioxane in the spectra also does not change, though in the case of pure thermal mechanism of POM decomposition, increase in the contribution of the intensity of oxymethylene would be expected, since oxymethylene is the only product of POM mass-spectrum upon pure thermal decomposition [4] at the same sensitivity of the registration channel of mass-spectrometer. It can be assumed that the absence of strong increase in the intensity of decomposition products in POM-POM pair in vacuum upon long friction time after $F^{min}_{fr} \rightarrow F^{max}_{fr}$ transition might indicate specific and not yet understood behavior of the friction interface at melting point which can alter its thermal characteristics. This might be accounted for in further development of the simplified thermal model we use by considering heat effects associated, e.g., with formation of active macroradicals in air and vacuum as well as other concomitant phenomena.

In asymmetric friction pairs (e.g. polymer-steel) described above in the previous section in terms of *I*-*W* plots, the distribution of tribogenerated energy into contacting bodies can be described by a heat distribution coefficient k_d not equal to 0.5 used in our calculations of symmetric pairs POM-POM and PTFE-PTFE. The calculation shows that change in the value of k_d by ~ 5 % can lead to a change in the heating level at the interface by ~ 10 K. This issue can become important in the study of heterogeneous friction pairs where the macromolecular scissions and the related change in wear observed in POM-POM pair would be found. Note additionally, in the case of asymmetric pairs the polymer transfer layer may continuously change the heat transfer coefficient (e.g. for steel-PTFE pair the qualitative estimate of Sharron formula gives high k_d value of ~ 0.9 [23]) towards the k_d ~ 0.5 value for symmetric pair. This requires additional modifications of the model not yet considered in the current work. In this regard note, that in the work [5] we presented the data on friction and wear of POM against polyetheretherketone (PEEK). PEEK has thermal properties close to those of POM. Thus, k_d in this pair is expected to be close to 0.5. Nonetheless, the effects we observed in [5] for POM-PEEK pair are similar to those we observe in this work in the case of polymers sliding against steel, i.e. stable behaviour of friction force, absence of the $F^{min}_{fr} \rightarrow F^{max}_{fr}$ transitions characteristic for POM-POM pair, absence of the dependence of *I* on *W* and absence of the decomposition products of both POM and PEEK. This additionally implies that friction force transitions and the related wear behavior are rather dependent on the molecular mechanisms initiating scission of macromolecules and are dependent on the nature of the polymers in contact.

The calculated maximum heating temperatures in PTFE-PTFE pair in air conditions for typical value of μ ~ 0.1 are strongly lower than in POM-POM pair at the same initial (before $F^{min}_{fr} \rightarrow F^{max}_{fr}$ transition in POM-POM pair) level of *W*. This is due to around three times higher μ in POM-POM pair after $F^{min}_{fr} \rightarrow F^{max}_{fr}$ transition. E.g., for initial levels of *W* of ~ 0.03 MW/m^2, calculated heating temperatures at the interface during friction under atmospheric conditions exceed values of ΔT ~ 400 K for POM-POM pair (not shown) compared to ~ 200–300 K in PTFE-PTFE pair (Fig. 4(c)). Heating at the level of ΔT ~ 400 K already corresponds to temperatures of intense thermal decomposition of POM macromolecules [4], but are somewhat lower than similar temperatures for PTFE (see analysis of the thermal decomposition spectra of a number of depolymerizing polymers in [35]). The absence of friction force transitions in PTFE-PTFE, steel-POM, and steel-PTFE pairs and the absence of thermal decomposition products of these polymers

during friction of these pairs in vacuum measured in [4,5] may indicate that wear of these pairs in vacuum at the levels of W used in these works (up to ~ 0.005 MW/m^2) is not a consequence of tribo-induced ruptures of macromolecules or of their pure thermal decomposition and have, thus, pronounced mechanical nature.

The use of higher initial W values requires more advanced technical means of friction realization in vacuum. It is to note, with this regard, that the example of friction force measurements with PTFE-PTFE pair (W ~ 0.02 MW/m^2) in atmosphere conditions shown in Fig. 4(c) corresponds to V value five times higher than those used up to now in our vacuum measurements [4,5]. It is seen from the figure, that, similar to the case of POM-POM pair discussed above, the experimentally measured temperature dependence at measurement point is best fit by using simulated curve for experimentally measured $F_{fr}(t)$ and for h = 8 Watt/(m^2·K) (Fig. 4(c), curve 2). The simulations with other values of h are described in figure captions. As is seen, at this high sliding velocity, FEM calculations for h = 0 Watt/(m^2·K) predict that heating of PTFE-PTFE interface in vacuum would attain ~ 600 °C (curve 4, Fig. 4(c)), that is, the temperatures of intense thermal decomposition of PTFE [35]. This would imply the formation of large quantities of PTFE monomer: tetrafluoroethylene. Experimental verification of this prediction awaits further experimental research.

Conclusions

1. In order to quantify experimentally measured friction generated temperatures and predict the temperatures at the friction interface from the measured friction force dependences, finite elements simulations in realistic thrust bearing geometry used in the study have been developed with account for atmospheric and vacuum conditions via heat convection coefficients.
2. The simulation approach is shown to give significant improvements in the accuracy of the temperature calculations compared to analytical solutions. The approach provides the estimate of the heating level required to initiate triboinduced scissions of POM macromolecules observed *via* the mass-spectrometric registration of the triboinduced volatile products, differing from those registered upon pure thermal decomposition of POM. This level is estimated to be below the temperatures of melting and intense thermal decomposition of POM, thus supporting triboinduced nature of bond scissions. The absence of the increase of the decomposition products formation in the friction regimes at simulated heating level corresponding to the intense thermal decomposition of POM above melting point of this polymer suggests that the mechanism of pure thermal decomposition of macromolecules cannot explain the wear behavior in POM-POM pair and requires the presence of triboinduced scissions of macromolecules formed at the early stages of friction upon friction force transition from low to high level.
3. The simulations are in good accord with the exponential dependence of energetic wear on the level of friction force power observed in the case of friction of POM-POM and absence of changes of energetic wear with friction power in other pairs studied. The energetic wear of polymer-polymer and polymer-steel pairs not accompanied by scissions of macromolecules and friction force transitions (PTFE-PTFE, POM-steel, PTFE-steel) is shown to be independent on the level friction power and on the triboinduced heating. The

energetic wear in these pairs was obtained to be: I ~ 1 g/MJ (PTFE-PTFE), ~ 10 g/MJ (steel-PTFE) and I ~ 0.03 g/MJ (steel-POM). In the POM-POM pair before friction force transition, associated with macromolecular bond scissions, the wear of POM was below sensitivity of the balances used. It might be thus suggested that I before friction force transition in POM-POM pair also does not depend on friction power and might be estimated to not exceed the level of the lowest value registered in the study of ~ 0.03 g/MJ.

4. The approach developed provides new strategies and instruments for the research of practically important problem of friction and wear of polymers and their composites. For example, the approach has been shown to be informative in comparing wear of POM and its composite with fullerene.

References

1. Friedrich K, Schlarb AK. (eds.) *Tribology of Polymeric Nanocomposites*. Butterworth-Heinemann; 2008.
2. Yumashev A, Mikhaylov A. Development of polymer film coatings with high adhesion to steel alloys and high wear resistance. *Polymer Composites*. 2020;41(7); 2875–2880.
3. Chichinadze AV. (ed.) *Osnovi Tribologii (trenie, iznos, smazka)*. Moscow: Mashinostroenie; 2001. (In Russian)
4. Pozdnyakov AO. Formation of Decomposition Products of Macromolecules Upon Friction of Polymer Against Polymer. *Tech. Phys. Lett.* 2023;49: 108–111.
5. Pozdnyakov AO, Syanshun L, Sedakova EB. Molecular Mechanisms of Polyoxymethylene Wear. *Journal of Friction and Wear*. 2024;45(1): 24–31.
6. Persson BNJ. *Sliding Friction*. Verlag: Springer; 2000.
7. Conte M, Pinedo B, Igartua A. Frictional heating calculation based on tailored experimental measurements. *Tribol. Int.* 2014;74: 1–6.
8. Grzes P. Determination of the maximum temperature at single braking from the FE solution of heat dynamics of friction and wear system of equations. *Numerical Heat Transfer, Part A: Applications*. 2017;71(7): 737–753.
9. Grigoriadis K, Mavros G, Knowles J, Pezouvanis A. Experimental investigation of tyre–road friction considering topographical roughness variation and flash temperature. *Tribology International*. 2023;181: 108294.
10. Belhocine A, Abdullah OI. Finite element analysis (FEA) of frictional contact phenomenon on vehicle braking system. *Mechanics Based Design of Structures and Machines*. 2020;50(9): 2961–2996.
11. Nosko O, Tsybrii Yu. Inverse determination of sliding surface temperature based on measurements by thermocouples with account of their thermal inertia. *Tribology International*. 2021;164: 107200.
12. Frankel JI, Chen H. Analytical developments and experimental validation of a thermocouple model through an experimentally acquired impulse response function. *International Journal of Heat and Mass Transfer*. 2019;141: 1301–1314.
13. Roda-Casanova V, Fernandes CMCG. A comparison of analytical methods to predict the bulk temperature in polymer spur gears. *Mechanism and Machine Theory*. 2022;173: 104849.
14. Nosko O, Tsybrii Y, Torrelio Arias TPG, Senatore A. Temperature Measurements at Tyre Tread Rubber on Sandpaper Oscillatory Sliding Contacts Using Acicular Grindable Thermocouples. *Tribol. Lett.* 2024;72: 75.
15. Roda-Casanova V, Sanchez-Marin F, Martinez-Cuenca R. Convective heat transfer modelling in dry-running polymer spur gears. *International Journal of Mechanical Sciences*. 2023;241: 107927.
16. Vettergen VI, Bashkarev AY, Suslov MA. Kinetics of friction and wear of polymer composite materials. *Phys. Solid State*. 2005;47: 1681–1686.
17. Ratner SB, Lur'ie YG. The relation between wear and the thermochemical stability of polymers. *Polymer Science U.S.S.R.* 1966;8(1): 93–99.
18. Sivebaek IM, Samoilov VN, Persson BNJ. Frictional Properties of Confined Polymers. *Eur. Phys. J.* 2008;27: 37—46.
19. Mergler YJ, Schaake RP, Huis in't Veld AJ. Material transfer of POM in sliding contact. *Wear*. 2004;256(3–4): 294–301.
20. Jia BB, Liu XJ, Cong PH, Li TSh. An investigation on the relationships between cohesive energy density and tribological properties for polymer–polymer sliding combinations. *Wear*. 2008;264(7-8): 685–692.
21. Laux KA, Schwartz CJ. Effects of contact pressure, molecular weight, and supplier on the wear behavior and transfer film of polyetheretherketone (PEEK). *Wear*. 2013;297(1–2): 919–925.

22. Samyn P, Baets PD. Friction and wear of acetal: A matter of scale. *Wear*. 2005;259(1–6): 697–702.
23. Sedakova EB, Kozyrev YuP, Thermal distribution in the PTFE–steel frictional pair. *Russ. Engin. Res.* 2016; 36: 727–730.
24. Privalko VP. The glass temperature of polytetrafluoroethylene and polyoxymethylene. *Polym. Sci. U.S.S.R.* 1976;18(6): 1392–1397.
25. Brandrup J, Immergut EH, Grulke EA. *Polymer Handbook. Two Volumes Set 4th ed*. Wiley; 1989.
26. Fourier JB. *The Analytical Theory of Heat*. The University Press; 1882.
27. Lykov AV. *Theory of Thermal Conductivity*. Moscow: Higher School; 1967. (In Russian)
28. Gallager R. *Metod Konechnih Elementov: Osnovi*. Moscow: Mir; 1984. (In Russian)
29. Desai YM, Eldho TI, Shah AH. *Finite Element Method with Applications in Engineering*. Pearson Education India; 2011.
30. Galerkin BG. *Beams and plates. Series in some questions of elastic equilibrium of beams and plates*. Vestnik Ingenerov; 1915. (In Russian)
31. Stephen W. *Fundamental Principles of Heat Transfer*. New York: Pergamon Press; 1977.
32. Janahmadov AK. *Analysis of the Fractal Structure of Rough Friction Surfaces to Establish Transient Regimes of Frictional Contact*. *J. Frict. Wear.* 2023;44: 391–396.
33. Kiselev AP, Lazarev VA. Bouncing of the load and radiation of sound in dry friction. *Tech. Phys.* 1997;42: 581–583.
34. Babici LM, Tudor A, Romeu J. Stick-Slip Phenomena and Acoustic Emission in the Hertzian Linear Contact. *Appl. Sci.* 2022;12: 9527.
35. Pozdnyakov AO, Ginzburg BM, Ivanov MA, Stepanov SV, Pozdnyakov OF. Studying polymer-on-metal friction by thermodesorption mass spectrometry. *Tech. Phys. Lett.* 2007;33: 462–465.

About Authors

Aleksei O. Pozdnyakov
Candidate of Physical and Mathematical Sciences
Senior Researcher (Ioffe Institute, Saint-Petersburg, Russia)
Senior Researcher (Institute for Problems in Mechanical Engineering of RAS, Saint-Petersburg, Russia)

Elena B. Sedakova
Doctor of Technical Sciences
Leading Researcher (Institute for Problems in Mechanical Engineering of RAS, Saint-Petersburg, Russia)